Published in Applied Optics 43, issue 8, 1683-1694, 2004
which should be used for any reference to this work

Tunable, oblique incidence resonant grating filter for telecommunications

Guido Niederer, Hans Peter Herzig, Joseph Shamir, Hans Thiele, Marc Schnieper, and Christian Zschokke

We have designed a tunable, oblique-incidence resonant grating filter that covers the C band as an add–drop device for incident TE-polarized light. We tune the filter by tilting a microelectromechanical systems platform onto which the filter is attached. The fabrication tolerances as well as the role of finite incident-beam size and limited device size were addressed. The maximum achievable efficiency of a finite-area device as well as a scaling law that relates the resonance peak width and the minimum device size is derived. In good agreement with simulations, measurements indicate a negligible change in shape of the resonance peak from 1526 nm at a 45° angle of incidence to 1573 nm at a 53° angle with a full width at half-maximum of 0.4 nm. In this range the shift of the peak wavelength is linear with respect to changes in the angle of incidence.

1. Introduction

Resonant grating filters (RGFs) have recently attracted the attention of many research groups.[1] An RGF that consists of only a few homogenous dielectric layers combined with a grating can exhibit an extremely narrow reflection spectral band that otherwise would require a large number of uniform layers. Therefore RGFs are well suited for free-space filtering applications. However, they suffer from polarization dependence. A few configurations that included a one-dimensional grating[2] as well as crossed gratings[3] were proposed to achieve polarization independence. The design described in this paper is optimized for TE polarization. The working principle of a reflection RGF, or guided-mode resonance filter, is that a part of the incoming light is trapped through evanescent grating coupling into the waveguide. Destructive interference for the transmitted waves is obtained within a limited range of parameters, thus forming a resonance region. Outside this resonance region the light does not couple into the waveguide and is transmitted and reflected as from a regular stratified layer. With these techniques it is possible to design reflection and transmission filters.[4] In reflection filters, only a small part of the spectrum is reflected and the rest is transmitted. We focus on reflection filters because it is easier to achieve broadband transmission than broadband reflection with only a few homogeneous layers.

In this paper we describe the modeling and characterization of a RGF for use in a tunable drop device. We address the most important aspects for use with a microelectromechanical-system-based microsystem (tilting microelectromechanical systems platform[5]), such as the influence of the limited sizes of the incident beam and device, fabrication errors, and the dependence of the dispersion of the tilt angle on the device's performance. Our goal is to design, fabricate, and characterize a tunable RGF for telecommunications applications that cover the C band. In contrast to many RGF devices that work at normal incidence, ours is used for oblique incidence, [i.e., angle of incidence (AOI) near 45°]. This choice makes it easier to separate the incident and the reflected beams and facilitates the development of a tunable device as the resonance peak shape is maintained over the whole tuning range.

The organization of this paper is as follows: In Section 2 we describe the chosen RGF in an approximate simple model to gain physical insight. In Sec-

G. Niederer (guido.niederer@unine.ch), H. P. Herzig, and J. Shamir are with the Institute of Microtechnology, Rue A.-L. Breguet 2, 2000 Neuchâtel, Switzerland. H. Thiele, M. Schnieper, and C. Zschokke are with the Centre Suisse d'Electromagnetique et de Microtechnique SA, Badenstrasse 569, 8048 Zürich, Switzerland. J. Shamir is also with the Department of Electrical Engineering, Technion—Israel Institute of Technology, Haifa 32000, Israel.

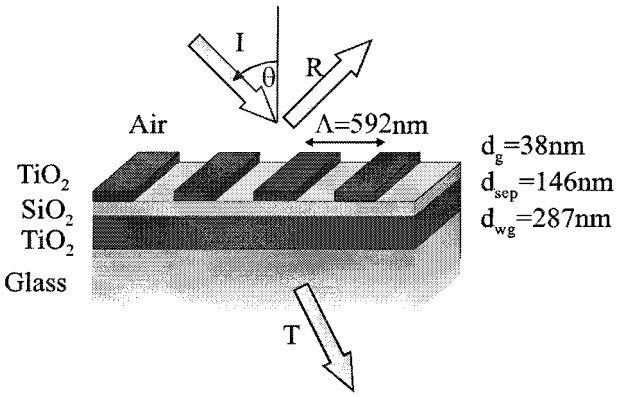

Fig. 1. RGF consisting of three layers. Thicknesses d are given. The assumed refractive indices are $n_{\mathrm{TiO_2}} = 2.298$, $n_{\mathrm{SiO_2}} = 1.444$, and $n_{\mathrm{Glass}} = 1.51$. The grating is rectangular, with a fill factor of 0.513.

tion 3 we present the design method and its application to our filter, including tolerancing, based on rigorous calculations by use of the Fourier modal method (FMM). The potential for miniaturization of the device is addressed in Section 4, in which the effects of the limited size of the device and the incident beam are considered. Experimental results obtained with the RGF that we fabricated are presented and compared with the model in Section 5, and concluding remarks are given in Section 6.

2. Simplified Model with Separate Treatment of the Grating and the Waveguide

Using the simple model presented below, we hope to arrive at a good approximate design for optimization by using rigorous methods as well as to obtain some insight into the basic coupling mechanisms. The model includes a grating that is separated from a planar waveguide by a low-index separation layer, as shown in Fig. 1. Thus, in this approximation, we may assume that the mode shape of the waveguide is not perturbed by the grating. The separation layer is chosen to have a refractive index that is lower than the waveguide to give good confinement in the waveguide, which produces evanescent coupling of the incoming light into the waveguide.

The well known equations[6] of a planar waveguide (self-consistency or transverse resonance condition) are

$$h_{\mathrm{wg}} k_0 n_{\mathrm{wg}} \cos(\theta_m) - \phi_c - \phi_s = m\pi, \tag{1}$$

$$n_e = n_f \sin(\theta_m), \tag{2}$$

where h_{wg} is the waveguide thickness; k_0 is the wave number in vacuum; n_{wg}, n_s, and n_c are the respective refractive indices of the waveguide, the substrate, and the cover; θ_m is the propagation angle in the waveguide; ϕ_c and ϕ_s are the phase shifts induced by total internal reflection at the cover and the substrate, respectively; m is the order of the mode, and n_e is the effective refractive index of the mode. The phase of the total internal reflection depends on the polarization, thus causing the device to be polarization dependent. Dealing only with the fundamental mode ($m = 0$), we suppose that $n_s > n_c$; then the waveguide supports only the fundamental mode when (cutoff conditions)

$$\text{for TE} \quad \frac{h_{\mathrm{wg}}}{\lambda} \le \frac{1}{2\pi\sqrt{n_f^2 - n_s^2}} \arctan\left(\frac{n_s^2 - n_c^2}{n_f^2 - n_s^2}\right) + \frac{1}{2\sqrt{n_f^2 - n_s^2}}, \tag{3}$$

$$\text{for TM} \quad \frac{h_{\mathrm{wg}}}{\lambda} \le \frac{1}{2\pi\sqrt{n_f^2 - n_s^2}} \arctan\left(\frac{n_f^4}{n_c^4}\frac{n_s^2 - n_c^2}{n_f^2 - n_s^2}\right) + \frac{1}{2\sqrt{n_f^2 - n_s^2}}. \tag{4}$$

For a given configuration and mode number the corresponding TM wavelength is always smaller than for TE, as $n_f > n_c$.

The grating coupler is governed by the following equation:

$$\frac{\Lambda}{\lambda_0}\left[n_{\mathrm{wg}} \sin(\theta_m) - n_{\mathrm{in}} \sin(\theta_{in})\right] = M, \tag{5}$$

where Λ is the grating period, λ_0 is the wavelength in vacuum, n_{in} is the refractive index of the incoming medium, θ_{in} is the angle of incidence in that medium, and M is the diffraction order. We prefer to write the grating equation [Eq. (5)] in this form because $n_i \sin(\theta_i)$ is a conserved quantity imposed by Snell's law. In our case we couple the incident light into the backward-propagating fundamental mode of the waveguide, which means that the sign of the angle in the waveguide, θ_m, is negative; it corresponds to the -1st diffraction order ($M = -1$). We are interested in maintaining only the 0th propagation order outside the waveguide to prevent unwanted diffraction losses. This is true when

$$\Lambda \le \frac{\lambda_0}{n_{\mathrm{in}} \sin(\theta_{\mathrm{in}}) + \max(n_{\mathrm{in}}, n_{\mathrm{out}})}. \tag{6}$$

Coupled Eqs. (1) and (5) can, unfortunately, not be solved in closed form. They have to be solved numerically. By fixing the geometry, the refractive indices of the materials, mode number m, and diffraction order M, we find, for every angle of incidence, a corresponding resonance wavelength, as long as the boundary conditions [Eq. (3) and inequalities (4) and (6)] are fulfilled. Thus we are led to a typical λ–θ map (dispersion map with λ, the resonance wavelength and θ, the corresponding AOI) that is valid for a specific polarization. The λ–θ map for $M = -1, m = 0, h_{\mathrm{wg}} = 287$ nm, $n_{\mathrm{wg}} = 2.298, n_s = 1.51$, $n_c = 1.444$, and TE polarization is shown in Fig. 2. For small variations of AOI θ near 45° the relation between the wavelength and the AOI is quite linear (Fig. 2, top). The waveguide in this example stays single mode for TE polarization for thicknesses in the

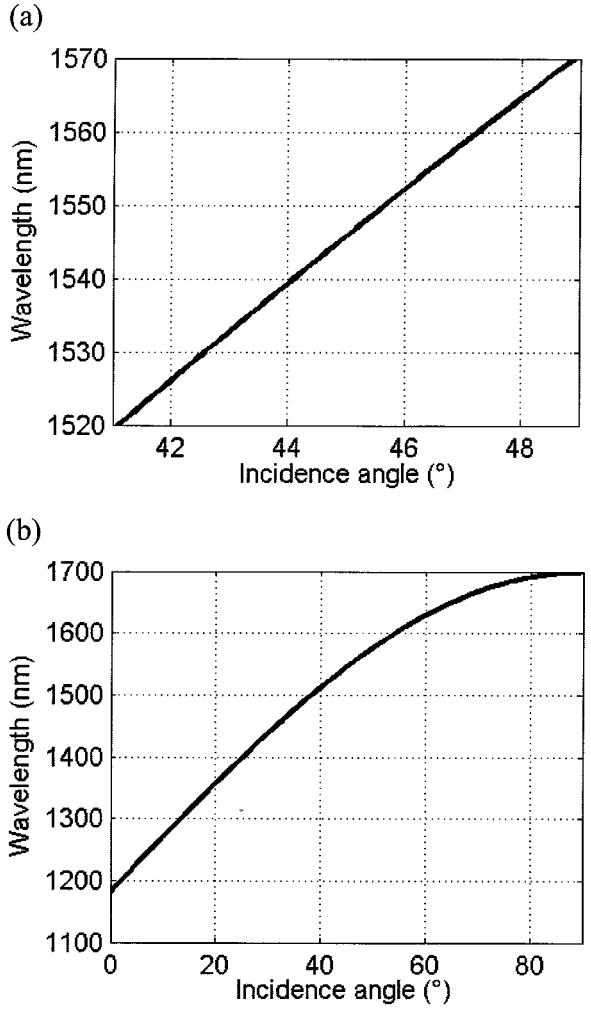

Fig. 2. λ–θ map based on the grating waveguide equations with $M = -1$, $m = 0$, $h = 287$ nm, $n_f = 2.298$, $n_s = 1.51$, and $n_c = 1.444$. (a) c band; (b) whole range of AOI.

range 53–455 nm, and inequality (6) gives a maximum period of 654 nm when the substrate material is taken as the outgoing medium (905-nm maximum grating period when the medium is surrounded by air).

3. Design

All calculations for the design of the filter are made by the FMM, sometimes also referred to as rigorous coupled-wave analysis.[7] The FMM deals with infinitely periodic structures in a harmonic expansion, with an incident field consisting of a superposition of plane waves. The effect of limited beam size and limited device size are investigated in Section 4 below. The structure investigated consists of three layers, as indicated in Fig. 1. The titanium dioxide (TiO_2) layer upon the glass substrate acts as the waveguide, whereas the silicon dioxide (SiO_2) layer—the separation layer—separates the waveguide from the grating that consists of the same material as the waveguide. From a fabrication point of view the separation layer forms an etch stop for the grating. The advantage of a noncorrugated waveguide is that the dispersion relation is close to linear, with a nearly constant resonance line width that is important for tuning applications.

The design procedure consists of several stages. First we have to choose the number of layers, the layer materials, the wavelength, and the AOI. For a symmetric peak shape and highest contrast, the structure has to be chosen to show a minimum reflection in the absence of resonance. For filtering applications we need shallow gratings (several tens of nanometers), and thus the grating height has only a small influence on the out-of-resonance response of the structure. Thus it is possible to fix the grating height and transform it, by means of effective-medium theory, into a homogenous layer to enable the layer thickness (waveguide, separation layer) to be determined for antireflection conditions. The reflectivity is a periodic function of layer thickness, so we choose the solution with the smallest thickness for single-mode operation. Afterward, the homogenous equivalent layer is transformed back to the grating, and we adjust the grating period to bring the resonance to the desired wavelength. The next step is to adjust the resonance linewidth. We can fix the resonance linewidth by changing the modulation strength of the grating. Now we have a good starting point for the fine tuning of the structure in an optimization routine. The resonance line shape for this kind of structure is Lorentzian.[8,9] If we are not at a reflectivity minimum, the reflection peak becomes asymmetric. It is meaningful to integrate the Lorentzian form directly into the merit function. The filter that results from this optimization routine is depicted in Fig. 1.

A. Summary of the Design Procedure

The steps in designing the tunable resonant grating filter are as follows:

1. Choose the structure (layers, materials, angle of incidence, wavelength).
2. Fix a reasonable grating height, such as an equivalent homogenous layer.
3. Solve for the thicknesses to fulfill antireflection conditions.
4. Determine the grating period to achieve resonance at the desired wavelength.
5. Change the grating height to get the desired FWHM.
6. Implement numerical optimization.

B. Tuning

The goal is to achieve a tunable resonant grating filter that covers the C band. We tune the filter by changing the AOI or tilting the filter. For better separation of the incident and reflected beams we operate at oblique incidence. The best way to show the filter's tunability is to plot the so-called λ–θ maps, where the reflection (or transmission) of the 0th order is plotted as a function of wavelength and angle of incidence. The sharp reflection peaks form a resonance line that corresponds to a given order of the

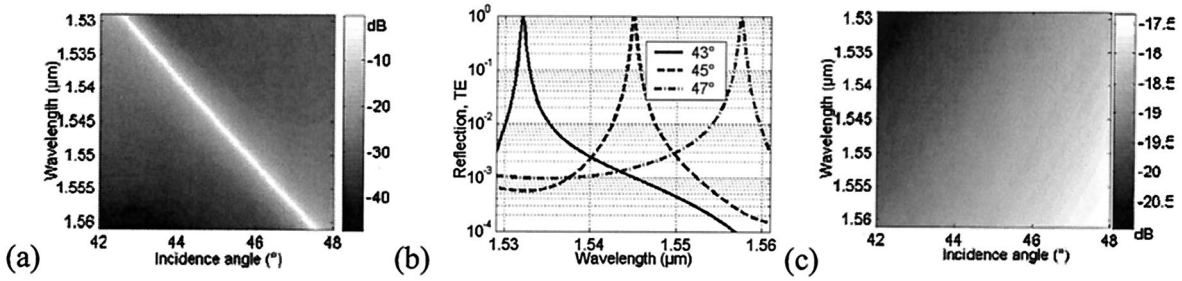

Fig. 3. Numerical results: (a) Reflectivity λ–θ map for TE polarization, (b) reflection spectra for three AOIs (TE polarization), (c) reflection λ–θ map for TM polarization (different scale).

waveguide. Because the grating is shallow, the rigorous λ–θ maps and the scalar calculations are similar as long as the grating modulation is not too strong, as they are not in our investigation. As can be seen from Fig. 3, it is sufficient to tilt the filter as much as 3° in both directions to cover the C band. The dependence of the resonance wavelength on the AOI is approximately linear, with a slope of 6.4 nm/°. A closer look, however, reveals a local slope variation from 6.7 nm/° at 42° to 6.1 nm/° at 48°. Furthermore, it can be seen that the resonance line shape stays almost constant over the whole tuning range, but its width changes from 0.472 nm at 42° (λ_{res} = 1525.0 nm) to 0.543 nm at 48° (λ_{res} = 1563.4 nm).

C. Fabrication Tolerances

For fabrication and characterization of the device it is important to know how the deviation of the design parameters influences the optical response of the device. Only a few papers[10,11] have evaluated the consequences of fabrication errors on filter performance. The target values of the reflection peak of our RGF are a full width at half maximum (FWHM) of 0.5 nm at a resonance wavelength of 1545 nm. From the optimization engine we get numbers with many digits. For an easy comparison we take the rounded values shown in Fig. 1, leading to a FWHM of 0.517 nm and a resonance wavelength of 1544.6 nm. The influences of the errors of the various design parameters on these two factors are listed in Table 1. The design values are listed in column 2 and the results of increasing these values by 3% on peak wavelength λ_{res} and on peak line width FWHM are given in columns 3 and 4, respectively. Except for the period and the high-index material, the influence on the resonance wavelength is significantly smaller than the relative change of the design parameter. In general, the relative effect on the linewidth is stronger than on the peak wavelength. For shallow gratings, some rules of thumb are known for the resonance linewidth[11] as a function of the grating height, the fill factor, and the modulation index.

An advantage of a tunable device is that a peak wavelength shift caused by fabrication errors can be compensated for by adjustment of the tilt angle.

D. Influence of Loss

The definition of loss in the waveguide community is the amount of light that is not guided further. Inasmuch as the amount of lost light is proportional to the total amount of light, it can be described by an exponential decay constant characterized by a total loss

Table 1. Tolerancing of Various Design Variables[a]

Parameter	Designed Value	Percentage Change of λ_{res} as a Result of +3% Increase of the Design Parameter	Percentage Change of FWHM as a Result of +3% Increase of the Design Parameter
Period (nm)	592	2.62	7.81
n_{TiO_2}	2.298	1.96	5.86
AOI (deg)	45°	0.55	3.28
d_{wg} (nm)	287	0.36	−6.86
$n_{substrate}$	1.51	0.22	−4.73
n_{SiO_2}	1.444	0.13	2.35
Fill factor	0.513	0.01	−0.51
$d_{grating}$ (nm)	38	0.00	5.87
d_{SiO_2} (nm)	146	0.00	−4.09
Amount of incomplete etching (nm)	3	−0.01	−14.83
Amount of overetching into SiO_2 (nm)	3	0.00	0.20

[a]The percentage changes of resonance wavelength λ_{res} and of resonance width FWHM (full width at half-maximum) that result from increasing the design parameter in column 2 by 3% are listed in columns 3 and 4, respectively. Values below 3% indicate an attenuation of the relative error in the optical response, whereas values above 3% indicate an amplification of the error. The device with the rounded design parameter shows a FWHM of 0.517 nm at 1544.6 nm at an AOI of 45°.

Table 2. Peak Reflection Efficiency of an Infinite Device as a Function of Absorption Loss Coefficient α of the Waveguide Material

Im (n)	α_{abs} dB/cm	FWHM (nm)	R_{max} (%)
0	0	0.517	100
1×10^{-6}	0.35	0.518	99.7
2×10^{-6}	0.71	0.519	99.4
5×10^{-6}	1.77	0.521	98.4
1×10^{-5}	3.53	0.526	96.8
2×10^{-5}	7.06	0.535	93.7
5×10^{-5}	17.66	0.561	85.3
1×10^{-4}	35.32	0.604	73.7

coefficient α_{tot}. The total loss coefficient can be written as the sum of the loss coefficients: scattering losses α_{sc}, radiation losses α_{rad}, and absorption losses α_{abs}. Assuming smooth interfaces, in the framework of this paper we neglect scattering losses. The radiation loss coefficient describes the interaction strength between the incident light and the light in the planar waveguide through the grating and is therefore proportional to the resonance linewidth of the structure.[12] As we desire a selective structure, we need weak coupling or a relatively small radiation loss coefficient. The relation of the radiation loss coefficient to the coupling length and its effect on finite devices are discussed in Section 4 below. In our case the unwanted loss is due to absorption and given by the absorption loss coefficient directly related to the imaginary part of refractive index $\alpha_{abs} = 4\pi/\lambda\ \mathrm{Im}(n)$. Rigorous calculations show that in the absence of absorption and scattering the peak reflection of resonant grating filters can reach 100% efficiency.[13] A quantitative overview of the reflection efficiency in the presence of absorption of the waveguide is given in Table 2.

4. Microsystems: Limited Size

Most treatments of RGF structures in the literature deal with infinite gratings that are not suitable for the microsystems of interest here. In this section we estimate the effects of finite dimensions on filter performance and derive the lower limit for proper operation. The approaches already described in the literature can be divided roughly into two classes: strong coupling devices with quasi-rigorous treatment[1,14,15] and weak coupling devices[16–19] with scalar and geometrical optics approximations.

To obtain a narrowband filter at oblique incidence, one must employ a weak coupling grating. Therefore, as is shown below, we need a large interaction length, which makes rigorous analysis difficult, and we have to apply some approximations. From simple physical considerations it is obvious that, for proper operation, the extended angular spectrum of a finite beam must fit within the limited angular range of the filter resonance. This issue is treated in Subsection 4.A and is followed by an investigation of the minimum filter length required to allow for adequate in-and-out coupling.

A. Finite Incident Beam and Angular Response of the Filter

This subsection applies only to oblique incidence. At normal incidence the situation is different. The slope of the dispersion map tends toward 0 at normal incidence. This is so because of the coexistence of two competing modes, which furthermore fulfill the Bragg condition for reflection within the waveguide. With doubly periodic structures, the angular tolerance can be increased even further.[20,21]

Assuming monochromatic illumination, the angular reflection response is directly related to the spectral reflection response through the slope of the λ–θ map at oblique incidence [Fig. 3(a)]. In the absence of absorption and scattering, a plane wave reaches 100% peak reflectivity at a given wavelength at the resonance angle. A mismatch of the resonance angle translates into a reduced peak reflectivity. A finite incident beam can be decomposed into plane waves (angular spectrum), and then each plane-wave component will have its specific reflection coefficient. The overall situation can be described by multiplication of the angular spectrum of the incident beam by the angular response of the filter. In spatial coordinates this is equivalent to a convolution of the incident beam with the Fourier transform of the angular response of the filter. We can see that the condition for high reflection efficiency is to guarantee that the incoming angular spectrum be smaller than the accepted angular spectrum of the resonant grating filter.

The incident beam distribution from a single-mode fiber collimator is assumed to be Gaussian and the angular response of the device is assumed to be Lorentzian. The angular response of the device is narrow in only one direction, the direction of the grating vector. Therefore we can limit the discussion to this one dimension.

Angular spectrum G of the incident Gaussian beam $g(x) = A_0 \exp[-(x/w)^2]$ with waist w is

$$G(p_x) = \mathrm{FT}\{g(x)\} = \sqrt{\pi}\ wA_0 \exp[-(\pi p_x w)^2], \quad (7)$$

where FT is a Fourier transform. We use the paraxial approximation, $p_x = x/\lambda z = \theta/\lambda$, to obtain the angle (in radians). When we are taking an angular offset of θ_0, the projections have to be taken into account. Then the angle in the paraxial approximation with angular offset has to be divided by $\cos(\theta_0)$ for use in the same formalism:

$$\begin{aligned} G(\theta) &= \sqrt{\pi}\ wA_0 \exp\left[-\left(\pi \frac{\theta w}{\lambda}\right)^2\right] \\ &= B_0 \exp\left[-\left(\pi \frac{\theta w}{\lambda}\right)^2\right], \\ G_{\mathrm{norm}}(\theta) &= \sqrt{\sqrt{2\pi}\,\frac{w}{\lambda}} \exp\left[-\left(\pi \frac{\theta w}{\lambda}\right)^2\right], \end{aligned} \quad (8)$$

where G_{norm} is the normalized angular spectrum of the Gaussian beam. We can see explicitly the well-known angular half-width at the $1/e$ points at $\theta =$

$\lambda/\pi/w$. Note that θ is the half-angle. The angular response of the RGF is of the Lorentzian type at oblique incidence in the absence of degenerate states, (i.e., no crossing lines in the λ–θ map). The optimized filter has an angular reflection response L with no offset (out of resonance reflection) and reaches 100% efficiency:

$$|L(\theta)| = \frac{(\Delta\theta/2)^2}{(\theta - \theta_{\text{offset}})^2 + (\Delta\theta/2)^2}. \quad (9)$$

Because the device will be tilted and here the angle is defined with reference to the incident beam, there will be an angular offset, $\theta \Rightarrow (\theta - \theta_{\text{offset}})$. The FWHM, $\Delta\theta$, is directly related to the slope of the λ–θ map with spectral linewidth $\Delta\lambda$: $\Delta\theta \doteq \Delta\lambda/\text{slope}$. Then the peak efficiency is given by[16]

$$\eta_B = \frac{\int |G(\theta)L(\theta)|^2 d\theta}{\int |G(\theta)|^2 d\theta} = \int [G_{\text{norm}}(\theta)]^2 |L(\theta)|^2 d\theta. \quad (10)$$

It should be reiterated that this is a simplified model. Incident angular spectrum $G(\theta)$ is real and positive. Because of this property, Eq. (10) is valid.

Our filter is designed to have a spectral FWHM of 0.5 nm and a slope of 6 nm/°. The output of a standard collimator has a waist of 0.5 mm. The simulated results are shown in Fig. 4: Fig. 4(a) shows a variable incident-beam diameter and a fixed linewidth of the filter and Fig. 4(b) shows a fixed incident-beam diameter with a variable linewidth. We can see that with our design values and a standard collimator we get a peak efficiency of only 64%. Note that for highly selective devices one has to choose either a wide collimated beam or reduced angular selectivity by maintaining the spectral selectivity, thus decreasing the slope of the λ–θ map.

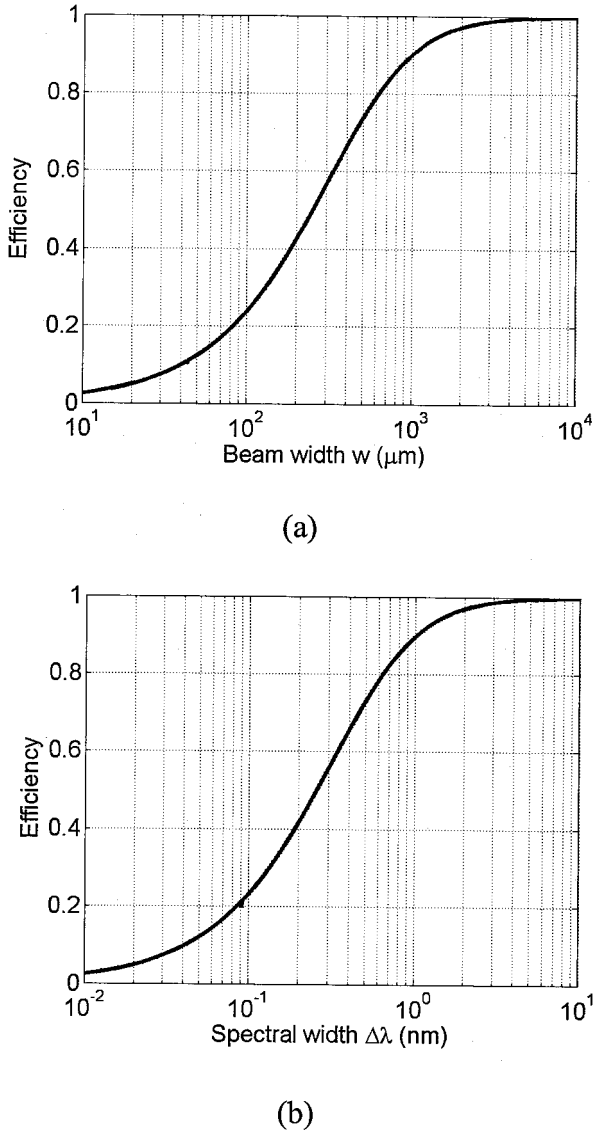

Fig. 4. Maximum peak reflectivity at $\lambda = 1.545$ μm with a slope of 6 nm/°: (a) fixed linewidth $\Delta\lambda = 0.5$ nm and slope with variable incidence beam waist, (b) fixed beam waist $w_0 = 0.5$ mm and slope with variable linewidth of the filter.

B. Limited Size of the Device

In principle, the minimum length of the filter is determined by the minimum interaction length of the grating that is sufficient for all the light to couple into the waveguide and couple out again. Any deviation from this requirement leads to reduced efficiency. We assume that we can divide the problem into two subproblems. First we have to determine the interaction strength of the grating, described by radiation loss coefficient α, or its inverse, coupling length L_c, and with this knowledge solve the differential equation that governs the energy exchange. There are approximate analytical expressions for the radiation loss coefficient for directly structured waveguides.[22,23] In our device the grating is separated from the waveguide by the separation layer, therefore this theory cannot be applied directly. To overcome this problem we may consider coupling as consisting of two processes, lateral grating coupling superimposed upon vertical evanescent coupling. The evanescent coupling through the separation layer can be described as a prism coupler. Qualitatively it can be said that, if the incident beam is much larger than the coupling length, there is almost no shift between the input and the output beams and we need, essentially, a device size of the order of the incident beam. The other extreme is that the coupling length is much longer than the beam size; thus incoupling is concentrated within a small area, which is followed by outcoupling governed by the exponential decay of the mode amplitude.

1. *Prism Coupler*

A simple way to couple into a planar waveguide is by use of evanescent wave coupling.[24] This can be achieved, for example, by illumination of a sandwich consisting of two high-index materials separated by a low-index material at an angle in the high-index ma-

terial that is large enough to cause total internal reflection at the first interface. The evanescent wave in the low-index material becomes a propagating wave in the second high-index material but with a decreased field amplitude, according to the exponential decay when the incident light passes through the low-index medium, that is governed by the decay constant. Decay constant α_e is simply the inverse of the penetration depth known from planar waveguide theory:

$$\alpha_e = k_0[n_{\mathrm{wg}}{}^2 \sin(\theta_m)^2 - n_c{}^2]^{1/2}. \tag{11}$$

With the parameters used in Section 2 and with $\lambda = 1545$ nm, angle θ_m is 56°, which leads to an exponential decay constant of $5.05 \times 10^6\ \mathrm{m}^{-1}$ or a penetration depth of 198 nm.

2. Grating Coupler

The period of our filter is short enough that only the -1st diffraction order is nonevanescent in the waveguide. Thus we get significantly simpler formulas.[21]

If we take a perfect planar waveguide with propagating light and add a semi-infinite grating at $z = 0$, the light will start to couple out by radiation. The field in the waveguide decreases exponentially with decay constant α_0, the radiation loss coefficient.

For a sinusoidally modulated waveguide of height h_{wg} with undulation amplitude $h_g/2$ within the Rayleigh approximation, the radiation loss coefficient for TE polarization can be expressed as[25]

$$\alpha_0 = \left(\frac{k_0 h_g/2}{2}\right)^2 \frac{n_{\mathrm{wg}}{}^2 - n_e{}^2}{n_e h_{\mathrm{wg}}} \frac{(n_{\mathrm{wg}}{}^2 - n_s{}^2)\{N_c N_{\mathrm{wg}}{}^2 + N_s[N_c{}^2 + (n_{\mathrm{wg}}{}^2 - n_c{}^2)\cos^2(N_{\mathrm{wg}} k_0 h_{\mathrm{wg}})]\}}{(N_{\mathrm{wg}}{}^2 + N_s N_c)^2 - (n_{\mathrm{wg}}{}^2 - n_c{}^2)(n_{\mathrm{wg}}{}^2 - n_s{}^2)[\cos^2(N_{\mathrm{wg}} k_0 h_{\mathrm{wg}})]}, \tag{12}$$

$$N_i = [n_i{}^2 - (n_e - \lambda_0/\Lambda)^2]^{1/2}, \qquad i = s, c, \mathrm{wg}, \tag{13}$$

where s, c, and wg correspond to substrate, cover, and waveguide.

With the same values as for the prism coupler and with a grating period of 592 nm we obtain $4620\ \mathrm{m}^{-1}$ for the radiation loss coefficient for the device without the separation layer, which corresponds to a coupling length of 217 μm.

Rectangular phase gratings couple more efficiently in the ± 1st order than a sinusoidal grating. The coupling strength of the grating is directly related to the spectral width of the resonance. Because Eq. (12) was derived for a sinusoidal grating we introduce a correction factor f_c to adjust the radiation loss coefficient for rectangular gratings. FMM calculations of the device of Fig. 1 with a rectangular grating and a fill factor of 0.5 show a linewidth of 0.518 nm, whereas with sinusoidal grating (sliced into 100 rectangles) and the same height they show a linewidth of only 0.322 nm. Thus $f_c = 0.518\ \mathrm{nm}/0.322\ \mathrm{nm} = 1.6009$.

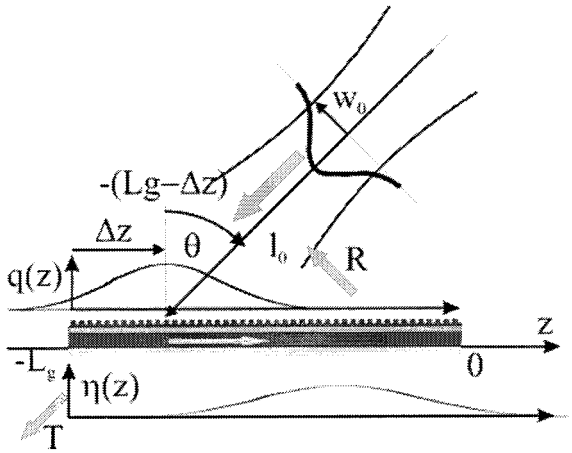

Fig. 5. Coupling model. A Gaussian beam with waist w_0 located at a distance l_0 from the grating hits the grating at $-(L_g - \Delta z)$ of the grating, described by complex amplitude $q(z)$ on the grating. The light couples in the backward direction of the waveguide and will be coupled out after some distance. Power efficiency $\eta(z)$ in the waveguide is the amount of power at z divided by the total incident power between $-L_g$ and z.

3. Combination of Prism and Grating Coupler

We know the interaction strength α_0 for a grating adjacent to the waveguide. But now the diffracted light has to tunnel twice through separation layer d_{sep}. Thus the equivalent radiation loss coefficient can be written as

$$\alpha = \alpha_0 f_c \exp(-2\alpha_e d_{\mathrm{sep}}). \tag{14}$$

With $\alpha_0 = 4620\ \mathrm{m}^{-1}$, $f_c = 1.6009$, $\alpha_e = 5.05 \times 10^{-6}\ \mathrm{m}^{-1}$, and $d_{\mathrm{sep}} = 146$ nm, we obtain $\alpha = 1701\ \mathrm{m}^{-1} = 1.701\ \mathrm{mm}^{-1}$.

4. Field Amplitude on the Grating

We adapt the formalism for the determination of the coupling efficiency,[25] with the difference that we do not try to maximize the light contained in the waveguide at the end of the grating of length L_g (Fig. 5). The device is illuminated by a Gaussian beam with waist w_0 at angle θ, with its center Δz away from the end of the grating. Waist w_0 of the Gaussian beam is located a distance l_0 from the grating. Then the normalized incident amplitude is given by[25]

$$q(z) = \sqrt{\frac{\sqrt{1/\pi}}{w_0}} \frac{1 + i\delta}{1 + \delta^2} \exp\left\{-\frac{i\delta}{1 + \delta^2}\left[\frac{z + \Delta z}{w_0/\cos(\theta)}\right]^2\right\} \times \exp\left\{-\frac{1}{1 + \delta^2}\left[\frac{z + \Delta z}{w_0/\cos(\theta)}\right]^2\right\}, \tag{15}$$

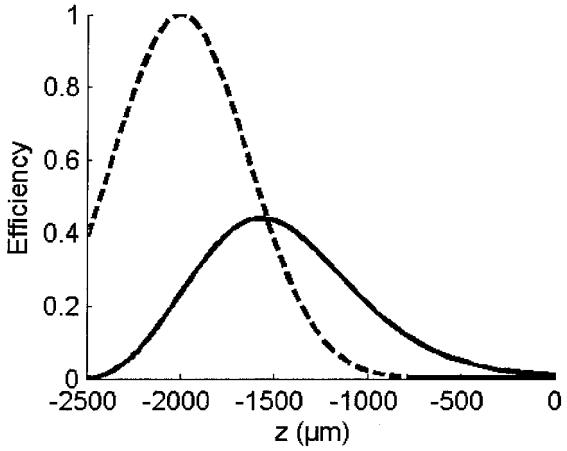

Fig. 6. Power efficiency $\eta(z)$ (solid curve) as a function of z on a finite device for a given incident beam. Dashed curve, normalized intensity of the incident beam $|q(z)|^2$. The simulation parameters are $w_0 = 500$ μm, $\Delta z = 500$ μm, $\lambda = 1545$ nm, $\alpha = 1.70$ mm^{-1}, and $\theta_0 = 45°$. Through the truncation of the incident beam we lose 8% of the energy. At $z = 0$ μm, after 2.5 mm we still have 4.4% of the light in the waveguide.

with

$$\delta = \frac{2[l_0 + (z + \Delta z)\sin(\theta)]}{k{w_0}^2}. \tag{16}$$

At normal incidence and with the waist on the grating, $\delta = 0$ and the complex amplitude reduces to a conventional Gaussian amplitude.

5. *Power Efficiency* η_{wg}

The power efficiency of the mode excitation, η_{WG}, is defined as the ratio between the power in the waveguide at a distance z and the incident power between $-\infty$ and z. The power in the mode of an infinite device is zero at $-\infty$, and light starts to couple in with the occurrence of the incident beam. After the power has reached its maximum, more light is coupled out than in. Far enough from the incident beam the light will be coupled out completely. Neglecting the scattering, absorption, and reflection at the edges of the grating yields an efficiency[25]

$$\eta(z) = 2\alpha\cos(\theta_0)\exp(-\alpha z)\left|\int_{-L_g}^{z}\exp[(\alpha + i\Delta\beta)z']q(z')\mathrm{d}z'\right|^2, \tag{17}$$

with

$$\Delta\beta = k(\sin\theta_0 - \sin\theta). \tag{18}$$

$\Delta\beta$ is the detuning from the excitation resonance. Maximal coupling occurs under synchronism condition $\Delta\beta = 0$, corresponding to the maximal power transport in the waveguide. An example of the power efficiency in the waveguide along the z axis is given in Fig. 6. For weak coupling gratings the shift

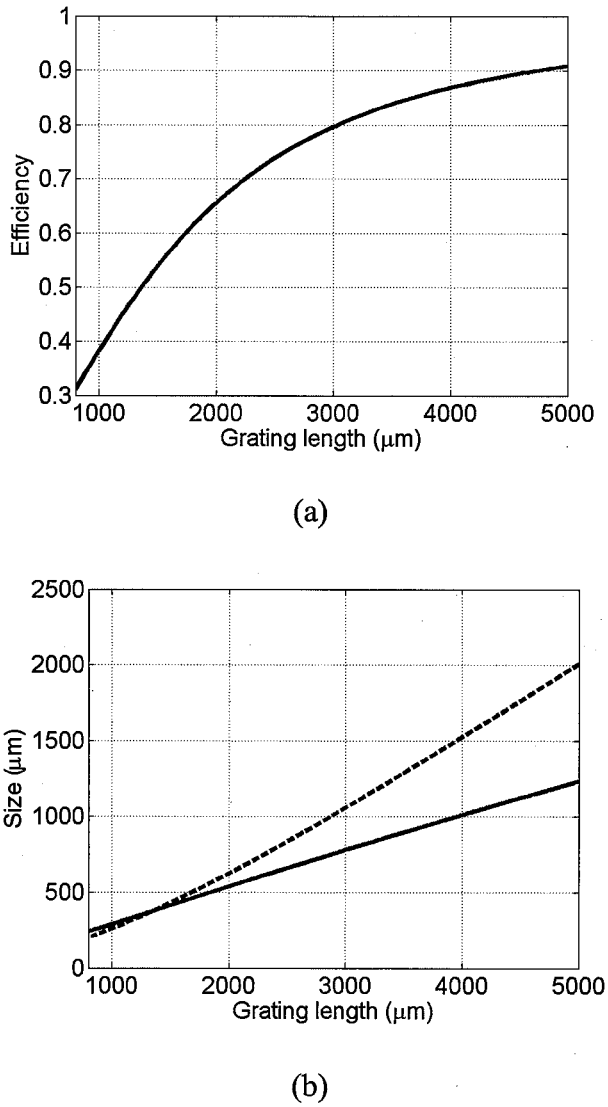

Fig. 7. (a) Maximum obtainable efficiency and (b) its corresponding width w (solid curve) and position Δz (dashed curve) as functions of grating length with coupling coefficient $\alpha = 1.70$ mm^{-1}.

Table 3. Simulations for a Device with Coupling Coefficient $\alpha = 1.70$ mm^{-1}[a]

Efficiency (%)	Grating Length	Gaussian Waist	Δz
30	0.765	0.234	0.194
40	1.024	0.296	0.268
50	1.360	0.380	0.380
60	1.724	0.471	0.515
70	2.228	0.596	0.719
80	3.012	0.788	1.064
90	4.720	1.173	1.871
95	7.133	1.693	3.061
98	12.067	2.682	5.534
99	17.900	3.784	8.464
99.5	26.500	5.328	12.778

[a]For a given efficiency in column 1 the minimum device length L_g is given in column 2. The corresponding Gaussian beam widths w and their positions at Δz are given in columns 3 and 4, respectively. All lengths are millimeters.

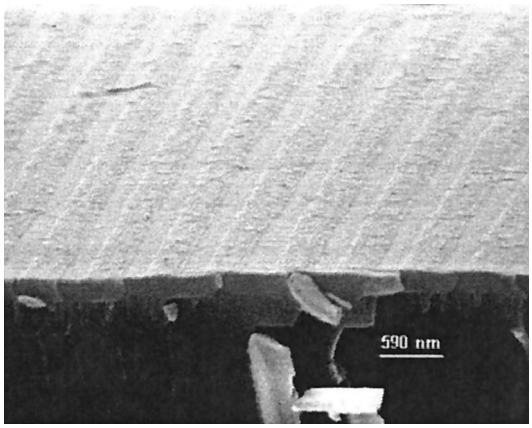

Fig. 8. Scanning-electron microscopy picture of the fabricated grating.

between the incident beam and the power in the waveguide is important and thus the decay in power efficiency in the tail is exponential because there is no longer coupling in.

C. Total Efficiency

The total efficiency (or maximum obtainable peak reflectivity) can be predicted as a function of the limited size of the system. The finite collimated incident beam (or minimum angular spread) leads to a maximum efficiency η_B [Eq. (10)]. The limited size of the device induces two kinds of loss, light not coupled out at the end of the device, $l_c = \eta_{\mathrm{wg}}$ [Eq. (17)] and light not impinging on the device, l_B:

$$l_B = 1 - \int_{-L_g}^{0} q(z)q^*(z)\mathrm{d}z. \tag{19}$$

Then we simply multiply the angular efficiency by the light coupled in and out to obtain the total efficiency η_{tot}:

$$\eta_{\mathrm{tot}} = \eta_B(1 - l_c - l_B). \tag{20}$$

For a given linewidth of the resonance peak, the coupling coefficient is fixed. We can maximize total efficiency η_{tot} by optimizing Gaussian beam width w and its position on the grating Δz for a given grating length L_g. From Fig. 7 we can see the maximum efficiency as a function of the grating length for a given coupling strength; some values are given in Table 3.

D. Scaling Law

For a given system with a specific efficiency we want to know how the system has to be scaled for a different spectral linewidth to get the same efficiency. For a given coupling coefficient (and thus a given linewidth) we derived an estimate of the maximum obtainable efficiency. Now we invert the problem and ask how the system dimensions have to be modified to produce the same efficiency for another linewidth. The simplest way is to keep the factors in Eq. (20) constant but with a different coupling coefficient.

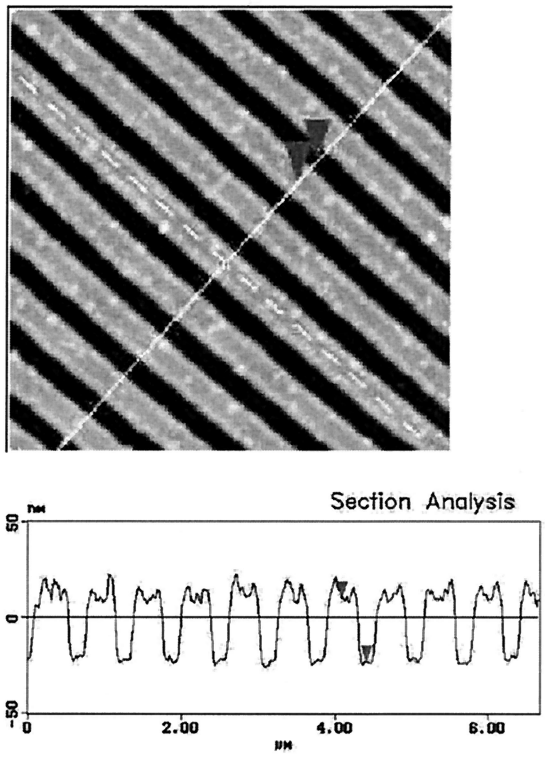

Fig. 9. Atomic-force microscopy picture and profile of the grating structure, revealing an average grating depth of 35 ± 2 nm.

First we look at l_c [Eq. (17)] at $z = 0$ and with $\Delta\beta = 0$. We introduce a scaling factor f ($f > 0$). All dimensions (L_g, w, Δz) are multiplied by f, whereas coupling constant α is divided by the same factor f. Then we make a variable substitution $z' => f \times z''$, and we find the initial equation, resulting in the same efficiency. Then we look more closely at Eq. (10). The angular linewidth of the angular response of the

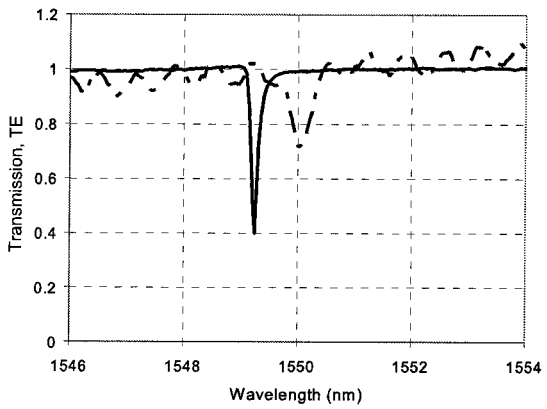

Fig. 10. Measured transmissivity of the device with the shallow (depth, 12 nm) grating measured with a big ($2w$ = 8-mm, solid curve) collimator at an angle of incidence of 49° and a small ($2w$ = 1-mm, dashed curve) collimator at an angle of incidence of 49.3°. The values are normalized to the offset of the Lorentzian curve fit. It is obvious that for the big collimator the hole is deeper and narrower than for the smaller collimator, which, owing to the measurement setup, shows undesirable Fabry–Perot interference fringes.

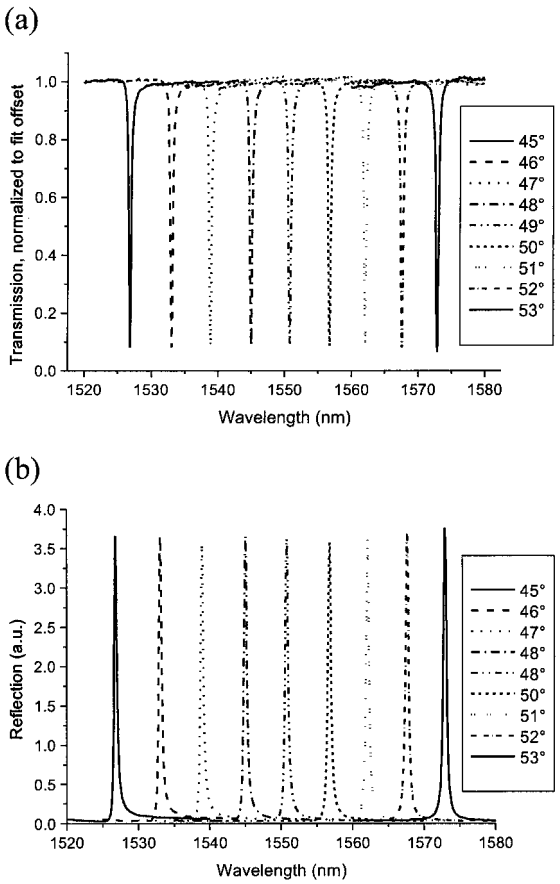

Fig. 11. Measured (a) transmission and (b) reflection spectra of the device with 35-nm grating depth. The transmission is normalized to the offset of the Lorentzian curve fit. The fit results are presented in Table 4. The collimator used for measurements is specified to have a beam diameter of 8 mm, and the sample size was 1 in. × 1 in.

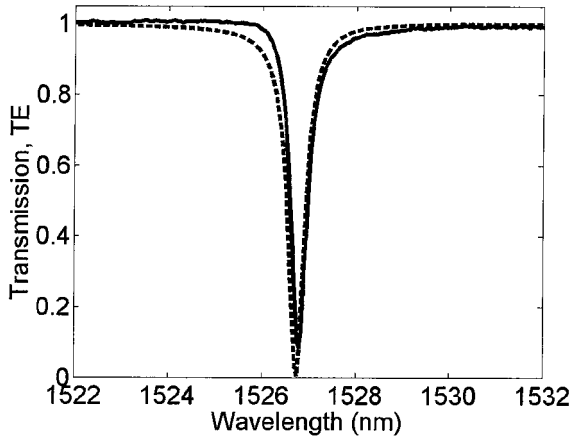

Fig. 12. Comparison of measurements and simulation. The measured values (solid curve) from Fig. 11 for a 45° AOI are compared with the simulated values (dashed curve), with n_{TiO_2} changed to 2.259.

filter is proportional to the spectral linewidth, determined by the slope in the λ–θ map. The angular width of the incident collimated Gaussian beam is inversely proportional to the width, w, of the beam. Thus, if we multiply w by factor f and divide the linewidth by f, we still obtain the same efficiency. At last we look at Eq. (19) and see that, if we scale the grating and the incident beam as well as their relative position by f, the same relative amount is lost. This knowledge results in the following scaling law: To increase the selectivity by a factor of f it is necessary to scale up the system by a factor of f''. This prediction is valid when absorption and scattering losses are neglected as well as fabrication errors, because they cannot be scaled. Thus for weak coupling devices the absorption will become a nonnegligible factor compared with the coupling coefficient. For our application this means that further reduction of the filter size while the linewidth is held constant will seriously reduce the peak efficiency.

5. Fabrication and Measurement Results

The resonant grating filter is fabricated in three successive process steps: deposition of the waveguide layers onto the substrate, holographic lithography to generate a grating structure on the layer stack, and finally etching of the grating. The deposition of the SiO_2 and TiO_2 layers is done by dc magnetron sputtering and optical monitoring of the achieved layer thickness. This standard procedure allows the layers to be deposited with ±3% tolerance error in optical thickness.

To begin construction of the grating structure we coat the layer stack with photoresist. For the holographic lithography a He–Cd laser beam (λ = 441.6 nm) is split into two beams, which interfere on the coated substrate to expose a linear grating with the desired 592-nm periodicity. Development of the photoresist results in a photoresist grating structure with a sinusoidal profile.

To transfer this grating into the topmost waveguide layer, we evaporate chrome onto the photoresist grating at an angle of incidence smaller than 45°. By careful adjustment of the angle of incidence and thickness of the chrome layer it is possible to generate a chrome grating with the same period as the grating in the photoresist and with a fill factor of 0.5.[26]

Subsequent etching of the resist with O_2 and of the upper waveguide layer with trifluoromethane (CHF_3) generates the desired rectangular grating structure in the waveguide layer. Finally, the remaining resist and chrome are removed. The final grating tolerances are defined by the achievable tolerances of the process steps: The grating period's accuracy is determined by holographic lithography and can be adjusted within a tolerance error well below 1%. The fill factor of the slope evaporated chrome grating is determined by the angle of incidence and the amount of chrome deposited as well as by the precision and depth of the photoresist sinusoidal grating. Practical tolerances are in the range ±0.1. The grating depth is determined by the etch rate of CHF_3 in the waveguide layer. As the material composition of TiO_2 (porosity) is critical not just for the refractive index of the layer but also for the etch rate, experi-

Table 4. Results of a Lorentzian Curve Fit of the Measured Reflection and Transmission Spectra at Several Angles of Incidence[a]

	Reflection Spectra			Transmission Spectra		
Angle (°)	λ_c (nm)	w (nm)	R_{max} (a.u.)	λ_c (nm)	w (nm)	ΔT_{max} (a.u.)
45	1526.80	0.40	3.71	1526.80	0.39	0.94
46	1533.04	0.43	3.74	1533.01	0.41	0.94
47	1538.92	0.44	3.59	1538.90	0.43	0.92
48	1545.01	0.45	3.72	1544.99	0.42	0.93
49	1550.80	0.46	3.71	1550.78	0.43	0.93
50	1556.77	0.47	3.64	1556.74	0.44	0.93
51	1562.10	0.47	3.68	1562.09	0.43	0.91
52	1567.63	0.48	3.79	1567.61	0.45	0.94
53	1572.93	0.49	3.88	1572.89	0.43	0.97

[a] R_{max} is the peak reflection and ΔT_{max} is the drop in transmission relative to the offset. The average slope between 45° and 53° AOI is 5.8 nm/°.

ments for a specific TiO_2 layer have to be performed to evaluate the exact etch rate.

Figure 8 shows a scanning-electron microscope picture of the final grating, which has a fill factor slightly larger than 0.5 and a still relatively rough TiO_2 surface; work is ongoing to improve these values. The corresponding atomic-force microscope picture, Fig. 9, of the same structure reveals a grating depth of 35 nm, close to the targeted 38 nm.

The diced filter sample was attached by index-matching oil to a wedge prism of 2° to prevent formation of parasitic Fabry–Perot interference fringes, and the assembly was mounted onto a precision rotation stage. The whole device is illuminated with a collimated beam from a modulated tunable laser source. The transmitted and reflected beam intensities are measured simultaneously by two detectors. As we are working in the 0th order and the material dispersion for this wavelength range can be neglected, it is possible to measure a spectrum from a certain AOI without readjusting the detectors. The orientation of the grating can easily be determined by illuminating the grating with a visible laser and creating the −1st diffraction order.

Experimental measurements were performed on two filters with different grating depths. The first filter sample had a grating depth of only 12 nm instead of the designed 38 nm. This resulted in a narrower and asymmetric resonance peak and a higher out-of-resonance reflectivity. It has to be mentioned that we used a Lorentzian fit to determine the width of the resonance peak even if the line shape was (slightly) asymmetric. Rigorous calculations show that the line width for the shallower grating drops from 0.52 to 0.052 nm without absorption or to 0.061 nm with $\alpha_{abs} = 0.8\ cm^{-1}$, accompanied by a significant drop in peak efficiency (from 100% to 75%). Assuming a slope of 6 nm/°, the spectral width of 0.06 nm corresponds to an angular width of 0.01°. The maximum peak efficiency [Eq. (10)], in this case for $\lambda = 1545$ nm and $w = 0.5$ mm, is only 10%, and for $w = 4$ mm it is 56%.

To investigate the filter's performance for various filter sizes and divergence angles of the collimated beam we measured the sample with a 12-nm grating with both (a) a large collimator ($2w = 8$ mm) and (b) a standard collimator ($2w = 1$ mm); see Fig. 10. As there is an uncertainty in the absolute normalization of the reflected beam we took the transmission spectra normalized by the offset of their Lorentzian fit to show the effect of a limited angular spectrum. The drop of the peak calculated from the fit was (a) 63.5% and (b) 30.0% with corresponding widths FWHM (a) 0.12 nm and (b) 0.33 nm. The predicted lower peak efficiency and its broadening were observed. The drop in the transmission spectrum includes not only the reflected part but the absorbed and the scattered parts as well.

The parameters of the other filter sample were closer to the design parameters with a grating depth of 35 nm, leading to the results of Fig. 11. The calculated peak reflection wavelength is 1544.4 nm; the peak width, 0.44 nm. The efficiency can be improved if the filter has close to the designed shape. The reflection peak at 45° AOI occurs at $\lambda = 1526.8$ instead of 1545 nm, with a line width of 0.4 nm. This shift toward shorter wavelengths, as well as the slight asymmetry, which diminishes for larger angles of incidence, can be attributed mainly to a smaller refractive index of the waveguide material than was assumed in the design. Therefore we simulated the transmission spectrum for an AOI of 45° with a lower index of refraction of TiO_2, namely, $n_{TiO_2} = 2.259$. The measured and simulated curves are shown in Fig. 12. The peak shift can be compensated for by an additional tilting of 3.0°, with no significant effect on the line shape. The same figure demonstrates that tuning over the full *C* band is feasible, as summarized in Table 4. The average tuning slope is 5.8 nm/°.

6. Conclusions

We have designed, fabricated, and characterized a simple three-layer tunable resonant grating filter for telecom wavelengths covering the C band with a FWHM of less than 0.5 nm. The concept of separating the grating from the waveguide leads to a linear dispersion relation for the waveguide in the region of interest, providing convenient tuning capability. An analysis of the effect of fabrication errors revealed that the peak position of this device is highly sensi-

tive to fabrication errors but that the peak shape is not. Thus additional tilting of the device places the resonance at the desired wavelength. Furthermore, we derived limitations for the miniaturization of the device by analyzing the influence on filter performance of a finite beam and a finite grating length. For an ideal, nonabsorbing device, the achievable width of the reflection peak for a given peak reflectivity is inversely proportional to the beam size and grating length. Obviously, the result in a real filter is a proportional increase of the sensitivity to absorption and fabrication errors with increasing filter selectivity.

The measured reflection and transmission curves are similar to the calculated curves. The reflection peak was shifted toward shorter wavelengths, rendering the peak shape slightly asymmetric. The shift of the peak can be compensated for by an additional tilt of 3°.

The authors acknowledge financial support from the Centre Suisse d'Electronique et de Microtechnique. Further, we thank O. Parriaux and his group at Université Jean Monnet, St-Etienne, France, for fruitful discussions.

References

1. See, for example, J. M. Bendickson, E. N. Glytsis, T. K. Gaylord, and D. L. Brundrett, "Guided-mode resonant subwavelength gratings: effect of finite beams and finite size," J. Opt. Soc. Am. A **18,** 1912–1928 (2001), and references therein.
2. D. Lacour, G. Granet, J. P. Pluemey, and A. Mure-Ravaud, "Polarization independence of a one-dimensional grating in conical mounting," J. Opt. Soc. Am. A **20,** 1546–1552 (2003).
3. A. Mizutani, H. Kukuta, K. Nakajima, and K. Iwata, "Nonpolarizing guided-mode resonant grating filter for oblique incidence," J. Opt. Soc. Am. A **18,** 1261–1266 (2001).
4. S. Tibuleac and R. Magnusson, "Reflection and transmission guided-mode resonance filter," J. Opt. Soc. Am. A **14,** 1617–1626 (1997).
5. T. Overstolz, P.-A. Clerc, M. T. Gale, H. P. Herzig, G. Niederer, W. Noell, J. Söchtig, H. Thiele, and N. F. de Rooij, "Tilting out-of-plane platform for optical applications," in *International Conference on Optical MEMS*, conference digest (Institute of Electrical and Electronics Engineers, Piscataway, N.J., 2002), pp. 81–82.
6. H. Kogelnik, "Theory of dielectric waveguides," in *Integrated Optics*, T. Tamir, ed. (Springer, New York, 1979), pp. 15–79.
7. M. G. Moharam and T. K. Gaylord, "Diffraction analysis of dielectric surface-relief gratings," J. Opt. Soc. Am. A **10,** 1385–1392 (1982).
8. D. Rosenblatt, A. Sharon, and A. A. Friesem, "Resonant grating waveguide structures," IEEE J. Quantum Electron. **33,** 2038–2059 (1997).
9. S. M. Norton, T. Erdogan, and G. M. Morris, "Coupled-mode theory of resonant grating filters," J. Opt. Soc. Am. A **14,** 629–639 (1997).
10. Z. Hegedus and R. Netterfield, "Low sideband guided-mode resonant filter," Appl. Opt. **39,** 1469–1473 (2000).
11. D. Shin, S. Tibuleac, T. A. Maldonado, and R. Magnusson, "Thin-film optical filters with diffractive elements and waveguides," Opt. Eng. **37,** 2634–2646 (1998).
12. I. A. Avrutsky and V. A. Sychugov, "Reflection of a beam of finite size from a corrugated waveguide," J. Mod. Opt. **36,** 1527–1539 (1989).
13. L. Mashev and E. Popov, "Zero order anomaly of dielectric coated gratings," Opt. Commun. **55,** 377–380 (1985).
14. J. Saarinen, E. Noponen, and J. Turunen, "Guided-mode resonance filters of finite aperture," Opt. Eng. **34,** 2560–2565 (1995).
15. K. Hirayama, E. N. Glytsis, and T. K. Gaylord, "Rigorous electromagnetic analysis of diffraction by finite-number-of-periods grating," J. Opt. Soc. Am. A **14,** 907–917 (1997).
16. E. Popov and B. Bozhkov, "Corrugated waveguides as resonance optical filters—advantages and limitations," J. Opt. Soc. Am. A **18,** 1758–1764 (2001).
17. R. R. Boye and R. K. Kostuk, "Investigation of the effect of finite grating size on the performance of guided-mode resonance filters," Appl. Opt. **39,** 3649–3653 (2000).
18. D. K. Jacob, S. C. Dunn, and M. G. Moharam, "Normally incident grating reflection filters for efficient narrow-band spectral filtering of finite beams," J. Opt. Soc. Am. A **18,** 2109–2120 (2001).
19. D. K. Jacob, S. C. Dunn, and M. G. Moharam, "Design considerations for narrow-band dielectric resonant grating reflection filters of finite length," J. Opt. Soc. Am. A **18,** 2109–2120 (2001).
20. F. Lemarchand, S. Sentenac, and H. Giovanni, "Increasing the angular tolerance of resonant grating filters with doubly periodic structures," Opt. Lett. **23,** 1149–1151 (1998).
21. A. Mizutani, H. Kikuta, and K. Iwata, "Wave localization of doubly periodic guided-mode resonant grating filters," Opt. Rev. **10,** 13–18 (2003).
22. O. Parriaux, V. A. Sychugov, and V. Tishchenko, "Coupling gratings as waveguide functional elements," Pure Appl. Opt. **5,** 453–469 (1996).
23. W. W. Rigrod and D. Marcuse, "Radiation loss coefficient of asymmetric dielectric waveguides with shallow sinusoidal corrugations," IEEE J. Quantum Electron. **QE-12,** 673–685 (1976).
24. T. Tamir, "Beam and waveguide couplers," in *Integrated Optics*, T. Tamir, ed. (Springer, New York, 1979), pp. 83–137.
25. N. M. Lyndin, O. Parriaux, and V. A. Sychugov, "Waveguide excitation by a Gaussian beam and a finite size grating," Sensors Actuators B **41,** 23–29 (1997).
26. M. Schnieper, M. T. Gale, C. Zschokke, and C. David, "Application and fabrication of subwavelength gratings," in *Diffractive Optics and Micro-Optics*, R. Magnusson, ed., technical digest, Vol. 75 of OSA Trends in Optics and Photonics Series (Optical Society of America, Washington, D.C., 2002), pp. 228–230.